Validation of a computationally efficient time-domain numerical tool against DeepCwind experimental data.

A.B.K. Pribadi
Maritime Technology Division, Ghent University, Belgium
G. Verao Fernandez
Coastal Engineering, Bridges and Roads Research Group, Ghent University, Belgium
I. Martínez-Estévez
Environmental Physics Laboratory, CIM-UVIGO, Universidade de Vigo, Spain
L. Donatini
Maritime Technology Division, Ghent University, Belgium
E. Lataire
Maritime Technology Division, Ghent University, Belgium

ABSTRACT: This paper presents the algorithm of a computationally efficient and reliable time-domain numerical tool capable of modelling floating wind turbine (FWT) platforms subjected to waves loads. Validation is performed against the experimental data of the DeepCwind semi-submersible. The platform's responses are modelled according to the Cummins' equation of motion using frequency-domain hydrodynamic coefficients. Convolution integral of the impulse response functions for radiation forces is modelled using the recursive approach. The Morison equation is implemented to account for the drift force and viscous damping induced by the large heave plate. Mooring lines are modelled according to the lumped mass approach using an adapted version of the open source code MoorDyn. Modifications are done to model the hydrodynamic forces in the mooring lines subjected to waves and currents. A comparison is performed against DualSPHysics externally coupled with the MoorDyn+. This work is a foundation to further develop an FWT design optimization tool.

1 INTRODUCTION

Since 2001, wind turbines installed all around the world have reached the cumulative capacity of 837 Giga Watt (GW) by 2021 with a Compound Annual Growth Rate (CAGR) of 7 % of new commissioning for the past 5 years (Lee & Zhao 2021). By the end of 2021, there are 48 GW of capacity in-operation that comes from the offshore wind energy globally, which almost doubled the capacity compared to the year of 2019 (Herzig 2022). Global Wind Energy Council (GWEC) projected additional capacities of 557 GW by the end of 2026 in which 91 GW comes from the offshore wind energy (Lee & Zhao 2021). There is a growing potential in the use of floating structures that would allow installation in deeper water depth to be more economically feasible. In Europe alone, it is projected to install over 7 GW of floating wind farms over the next decade (Ramírez et al. 2021). As of late 2020, more than 81% of the existing offshore wind turbines are supported by monopile foundation with only 0.2 % accounts for floating structures of spar-buoy, semi-submersible and barge (Ramírez et al. 2021). In the framework of the growing industry of floating wind turbines (FWT), the different floating structures have their advantages and downsides attributed to their physical characteristics. In 2011, 1:50 scaled model tests were performed in the Maritime Research Institute Netherlands (MARIN) ocean basin by the DeepCwind consortium for three different floating platforms: spar-buoy, tension leg platform (TLP) and semi-submersible (Dagher et al. 2013; Goupee et al. 2012; Koo et al. 2014). Two objectives were set for the tests: to identify the physical characteristics of different typical FOWT structures and to provide a benchmark data to validate numerical tools capable of simulating aero-hydro-servo-elastic problems (Dagher et al. 2013). From the model tests, it was found that the semi-submersible type induced the lowest bending moment at the tower base compared to the TLP and spar-buoy structures (Goupee et al. 2012). Additional tests were performed in 2013 for the semi-submersible platform with an adaption made to the turbine that is replaced by the one built by MARIN (Goupee et al. 2014), which has better correlation to the full-scale performance of the National Renewable Energy Laboratory (NREL) 5 MW turbine (Jonkman et al. 2009). The same DeepCwind semi-submersible with the NREL 5 MW reference turbine was used as a study case to perform code-to-code comparisons between different software packages in the Offshore Code Comparison Collaboration Continuation (OC4) project (Robertson, Jonkman, Masciola, et al. 2014; Robertson, Jonkman, Vorpahl, et al. 2014). Furthermore, the Offshore Code Comparison

Collaboration, Continued, with Correlation (OC5) project validated different numerical approaches and compared their accuracies in simulating the aero-hydro-servo-elastic problems of the DeepCwind semi-submersible (Robertson et al. 2017). The simulations in OC5 performed by 21 participants using different numerical tools shown that on average the mooring line tension is 20 % underpredicted. This can be acceptable at the early design stage, albeit it can be problematic when optimizing the system further. Phase I of the on-going Offshore Code Comparison Collaboration, Continued, with Correlation, and unCertainty (OC6) project addressed this issue by focusing on the non-linear hydrodynamic problems and removing the uncertainties that come from the turbine and mooring lines (Robertson et al. 2020).

In the past 10 years, the DeepCwind semi-submersible has been extensively studied by many researchers around the world mainly using potential-flow based software, Morison element model, hybrid approach of potential-flow based that includes Morison drag term (Coulling et al. 2013; Gueydon, Duarte, and Jonkman 2014; Hall and Goupee 2015; Robertson et al. 2017, 2020; Robertson, Jonkman, Vorpahl, et al. 2014); and recently higher fidelity hydrodynamics solver (Liu et al. 2017; Wang et al. 2022). The results of OC4 and OC5 suggest that modelling the mooring line dynamics provide superior results to the quasi-static approach, especially when the wave induced loads in line elements are included in the approach (Robertson et al. 2017). For this reason, in this paper the authors utilized a validated open-source mooring dynamic solver, "MoorDyn" (Hall and Goupee 2015), and made adaptations to include wave and current induced loads and horizontal seabed frictions model (Pribadi, Donatini, and Lataire 2019), here referred to as "Adapted-MoorDyn". Present paper includes a third variation of MoorDyn, further developed by UVIGO and referred to as "MoorDyn+". Furthermore, due to the large heave plate as well as considerable drift force, the use of hybrid-Morison model results in a better agreement than a potential-flow only approach. The hybrid-Morison approach implemented in this paper has been internally coupled with the Adapted-MoorDyn and validated against a moored cuboid (Fernandez et al. 2021). Further validation is needed especially against a more realistic floater geometry for the proposed method to be considered as reliable when modelling an FWT. For this purpose, the DeepCwind semi-submersible is chosen for the validation due to the numerous research previously done in the past decade, making it a robust study case. To compare the algorithm previously validated against a moored cuboid, the DualSPHysics (Domínguez et al. 2021) code is used, which is a Computational Fluid Dynamics (CFD) solver based on the Smoothed Particle Hydrodynamics (SPH) method. Specifically, the coupling between DualSPHysics and a mooring library presented in Domínguez et al. (2019), is used to perform the proposed comparison.

Going forward, the numerical approach presented in this paper will serve as an early design optimization tool to perform extensive number of simulations for different FWT mooring configurations, due to its time-efficient nature with reasonable accuracies for that purpose. In addition, simulations input/output will be utilized for surrogate model training. It was demonstrated that the use of surrogate model in mooring design optimization can reduce the computational cost by 114 times, albeit the author used 2500 mooring configurations for the training set of the surrogate model (Pillai, et al. 2019). Regardless, with the ever-growing number of different floating platforms design and their data availability, one can benefit from a machine-learning algorithm for mooring design optimization in the early design process.

2 NUMERICAL MODEL

This section explains the mathematical models and their assumptions used in the numerical tool. An open-source code called MoorDyn (Hall 2017; Hall and Goupee 2015) is adapted to be a stand-alone tool to simulate a moored floating rigid body used in this paper. Figure 1 shows the algorithm used in this approach. Firstly, the frequency domain calculations are performed. Then, based on the frequency domain coefficients; the added mass at infinity and impulse response functions (IRF) are obtained. The frequency domain excitation force, Prony's coefficients and infinite added mass are used as an input for the time-domain calculation, marked with a shaded rectangle in Figure 1. The internal coupling is done inside Adapted-MoorDyn solver to reduce

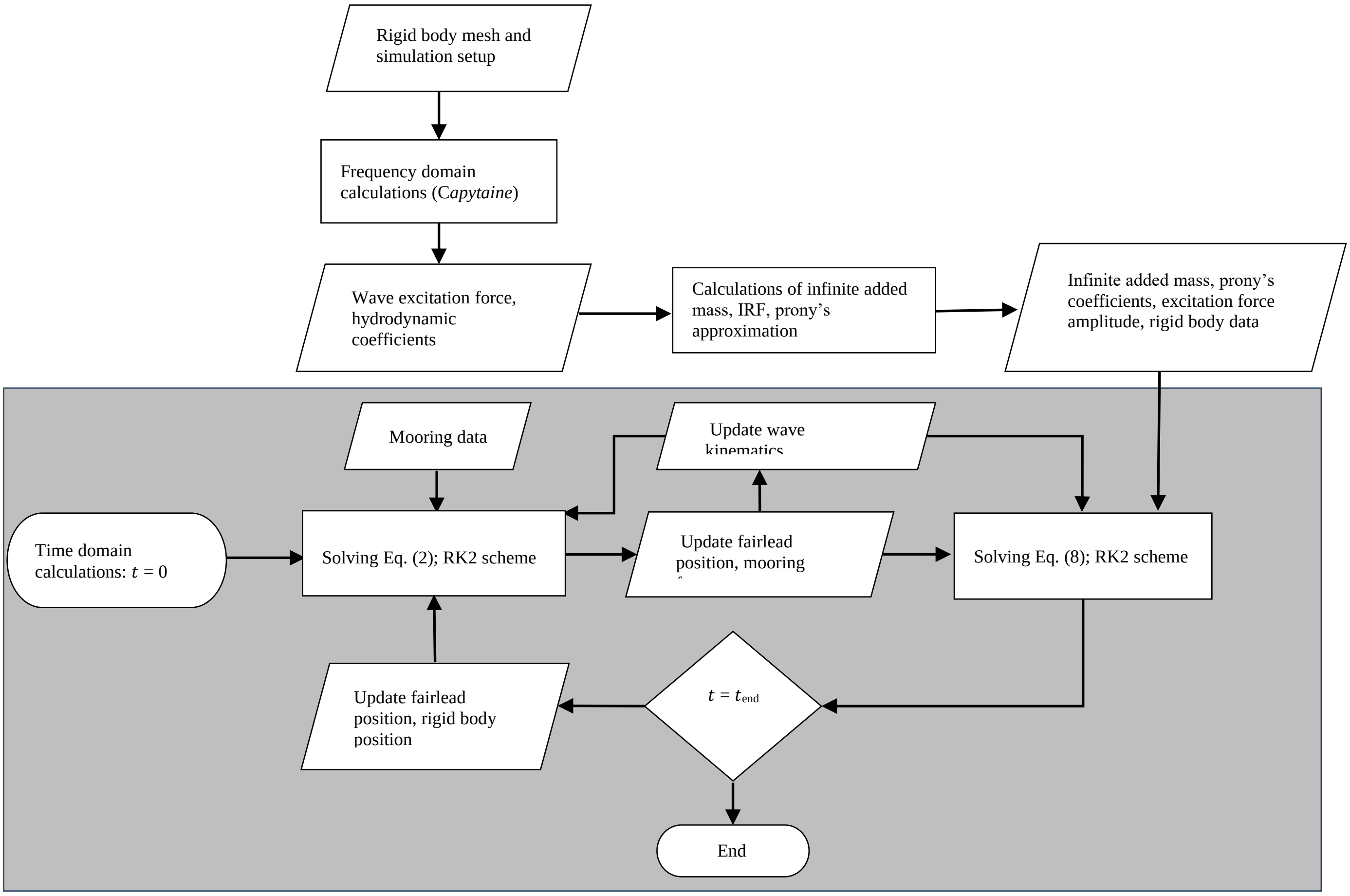

Figure 1. Flowchart of the algorithm used in this study

computational cost compared to the external coupling approach that the original MoorDyn was intended to be used (Hall and Goupee 2015). At the beginning of the time-domain simulation, the position of the rigid body is used to update the fairleads' position. Then, based on the new position of the fairlead, forces are calculated for the line element. The fairlead total force is transferred to the rigid body to include in the Cummins' equation and solved using a Runge-Kutta second order (RK2) explicit scheme, the same integration scheme used to march in time for the mooring lines. This process is repeated until it reaches a predetermined simulation end time.

2.1 *Mooring lines*

MoorDyn is a mooring line dynamic solver based on the lumped-mass approach to model the dynamics of mooring lines. Adaptions to MoorDyn were implemented as such that wave kinematics, calculated using the linear Airy theory (Airy and G.B 1841), are included in the Morison equation (Morison et al. 1950) to model the hydrodynamics of the lines. In addition, seabed contact in the horizontal direction is modeled to simulate the friction between the lines and the sea bottom. These additions to the original MoorDyn have been previously used to simulate a mooring system for a mussel longline where the modifications to the code is explained in details (Pribadi et al. 2019). A line is discretized into S number of segments with their internal and external forces transferred into S+1 number of nodes. A node receives half of the total force F_i transferred from its neighboring segment. The force F_i is the contribution of tension T, numerical damping C, weight W, buoyancy B and hydrodynamic forces from the Morison equation F_{drag} and $F_{inertia}$ (Fernandez et al. 2021; Morison et al. 1950; Pribadi et al. 2019). F_i is dependent on the node's position r_i, node's velocity $\dot{r}_i$, fluid's velocity v_i and fluid's acceleration $\dot{v}_i$, as shown in Equation (1):

$$F_i\big(r_i(t), \dot{r}_i(t), v_i(t), \dot{v}_i(t)\big) = F_{drag}\big(\dot{r}_i(t), v_i(t)\big) + F_{inertia}\big(\dot{v}_i(t)\big) + T\big(r_i(t)\big) + C\big(\dot{r}_i(t)\big) + W + B \tag{1}$$

Subscript i represents the spatial dimension of x, y and z. Note that $F_{inertia}$ takes only the contribution of fluid's acceleration as the contribution from line's acceleration is included in the left-hand-side of Equation (2). The node's acceleration $\ddot{r}_i$ at time t for a single node is calculated using the following equation:

$$(m + a)\ddot{r}_i(t) = F_i\big(\dot{r}_i(t), r_i(t), \dot{v}_i(t), v_i(t)\big) \tag{2}$$

where m = line segment's mass; a = line segment's added mass. Based on the Equation (2), a single node's positions $[r_x, r_y, r_z]$ and velocities $[\dot{r}_x, \dot{r}_y, \dot{r}_z]$ are obtained by constructing a system of Ordinary Differential Equations (ODEs) solved using the RK2 scheme. This is done by introducing a state vector X and a derivative of a state vector $\dot{X}$ shown in Eq. (3) and (4):

$$X(t) = \begin{bmatrix} \dot{r}_x(t) \\ r_x(t) \\ \dot{r}_y(t) \\ r_y\,(t) \\ \dot{r}_z(t) \\ r_z\,(t) \end{bmatrix} \quad (3) \qquad \dot{X}(t) = \begin{bmatrix} \ddot{r}_x(t) \\ \dot{r}_x(t) \\ \ddot{r}_y(t) \\ \dot{r}_y(t) \\ \ddot{r}_z(t) \\ \dot{r}_z(t) \end{bmatrix} \quad (4)$$

Suppose that the integration time-step of Δt is used. To obtain the state vector X at time $t + \Delta t$, RK2 scheme can be divided into two integration steps (Press et al. 2007). Firstly, total force F_i at time t is calculated using Eq. (1). Secondly, the node's accelerations are calculated using Eq. (2). Thirdly, derivative of a state vector $\dot{X}\ (t)$ is constructed by substituting Eq. (2) into (4):

$$\dot{X}(t) = \begin{bmatrix} (m + Ca)^{-1} F_x\big(\dot{r}_x(t), r_x(t), \dot{v}_x(t), v_x(t)\big) \\ \dot{r}_x(t) \\ (m + Ca)^{-1} F_y\left(\dot{r}_y(t), r_y\,(t), \dot{v}_y(t), v_y(t)\right) \\ \dot{r}_y(t) \\ (m + Ca)^{-1} F_z\big(\dot{r}_z(t), r_z\,(t), \dot{v}_z(t), v_z(t)\big) \\ \dot{r}_z(t) \end{bmatrix} \quad (5)$$

Then, the first numerical integration step is performed to calculate the state vector X at $t + \Delta t/2$ as follows:

$$X\left(t + \frac{\Delta t}{2}\right) = X(t) + \Delta t\, \dot{X}(t) \quad (6)$$

In the same manner as the previous steps, the total force F_i at time $t + \Delta t/2$ can be calculated to obtain $\dot{X}(t + \Delta t/2)$. Finally, the second part of RK2 scheme can be performed:

$$X(t + \Delta t) = X(t) + \Delta t\, \dot{X}\left(t + \frac{\Delta t}{2}\right) \quad (7)$$

By substituting (3) and (4) into (7), the positions and velocities of a single node at $t + \Delta t$ are obtained. Same principle applies to obtain the new positions of all S+1 number of nodes. In such case, the state vector and its derivate have the dimension of 6 x (S+1) as opposed to 6 shown in Eq. (3) and Eq.(4).

2.2 *Rigid body in Adapted-MoorDyn*

The method used to model the rigid body motions in this paper has been previously described in greater details (Fernandez et al. 2021) with a slight difference in the approach to calculate the viscous drag moment. As the hybrid approach is used, firstly, results from a separate potential-flow-theory based software are needed. In this case, an open-source boundary element method (BEM) solver Capytaine (Ancellin and Dias 2019) is used to obtain the results in the frequency domain. In the time-domain, the equation of motions of a rigid body in waves can be expressed using the Cummins' equation (Cummins 1962):

$$\begin{aligned}(\boldsymbol{M} + \boldsymbol{A}_\infty)\ddot{\boldsymbol{x}}(t) + \int_0^t \boldsymbol{K}_T\,(t-\tau)\dot{\boldsymbol{x}}(\tau)d\tau + \boldsymbol{K_h}\boldsymbol{x}(t) \\ = \boldsymbol{F}_{excitation} + \boldsymbol{F}_{viscous} + \boldsymbol{F}_{mooring}\end{aligned} \quad (8)$$

where $\boldsymbol{M}$ = rigid body's mass matrix; $\boldsymbol{A}_\infty$ = infinite added mass matrix; $\ddot{\boldsymbol{x}}(t)$ = rigid body's acceleration vector; and $\boldsymbol{K}_T$ = impulse response function (IRF) for the wave radiation forces; $\dot{\boldsymbol{x}}(t)$ = rigid body's acceleration vector; $\boldsymbol{K_h}$ = hydrostatic restoring matrix; $\boldsymbol{x}(t)$ = rigid body's position vector. The complex excitation force $\boldsymbol{F}_{excitation}$ is calculated as the summation of all directional spectral components utilizing the frequency-domain excitation force amplitude $\boldsymbol{f}_e$ and phase ε.

$$\boldsymbol{F}_{excitation} = \sum_{j=1}^{P}\sum_{l=1}^{Q} \zeta_{j,l}\ \boldsymbol{f}_e(\omega_j, \theta_l) e^{ik_j(x\cos\theta_l + y\sin\theta_l) + i(-\omega_j t + \varphi_{j,l} + \varepsilon_{j,l})} \quad (9)$$

where: j = frequency index; l = direction index; $\zeta_{j,l}$ = wave amplitude; ω_j= wave angular frequency; θ_l = wave direction; $\varphi_{j,l}$ = wave random phase; k_j = wave number.

$\boldsymbol{A}_\infty$ and $\boldsymbol{K}_T$ are calculated using the frequency domain coefficients (Ogilvie 1964) previously obtained from Capytaine. To reduce the computational effort, the convolution integral in Equation (8) is approximated using a recursive approach (Sheng, Alcorn, and Lewis 2015) shown in Equation (10) and (11):

$$\int_0^t \boldsymbol{K}_T\,(t-\tau)\dot{\boldsymbol{x}}(\tau)d\tau = \sum_{k=1}^{N} I_k\,(t) \quad (10)$$

$$I_k(t) = I_k(t - \Delta t)\, e^{\beta_k \Delta t} + \alpha_k e^{\beta_k \frac{\Delta t}{2}}\, \dot{\boldsymbol{x}}(t - \Delta t)\, \Delta t \quad (11)$$

where: α_k and β_k = Prony's coefficients (Duclos, Clément, and Chatry 2001); k = number of Prony's coefficients. This method is derived from the Prony's approach (Duclos et al. 2001) by evaluating and approximating the motion changes between two consecutive time steps. Thus, it is required to save the results of a previous time-step $I_k(t - \Delta t)$, which gets renewed on the next time step t. Compared to the direct convolution integral, this approach negates the need of saving and renewing all previous time history other than the one from a previous time-step $(t - \Delta t)$. In addition, unlike the conventional Prony's approach, this does not add extra ODEs to solve that can slow down the computational time, even compared to the direct integration method for higher number of degrees of freedoms (Armesto et al. 2015). As previously implemented, viscous effects are modelled using the drag term in the Morison equation (Fernandez et al. 2021). However, for the rotational degrees of freedoms, quadratic damping coefficient B_i^v is used instead:

$$F_{viscous} = \begin{cases} \frac{1}{2}\rho C_{D_i} A_i\big(v_i(t) - \dot{x}_i(t)\big)|v_i(t) - \dot{x}_i(t)|, & i = 1,2,3 \\ -B_i^v\big(\dot{x}_i(t)\big)|\dot{x}_i(t)|, & i = 4,5,6 \end{cases} \tag{12}$$

where C_{D_i} = drag coefficient; A_i = projected area; $\dot{x}_i(t)$ = rigid body's velocity; $v_i(t)$ = fluid velocity. The quadratic damping coefficients used in the calculations are described in the sub-section 3.1. The wave kinematics above calm water are calculated using Wheeler's approach (Wheeler 1970). To save computational time, wave dispersion relation is approximated using Fenton's approximation (Fenton 1988). Mooring force $F_{mooring}$ is transferred from the total force F_i at the fairlead node calculated in Equation (1). Finally, RK2 scheme is used to obtain the positions of the rigid body in time. This is done by turning the Equation (8) into a system of ODEs and solved in a similar manner as the mooring lines shown in the sub-section 2.1.

2.3 *Rigid body in DualSPHysics*

DualSPHysics is a fully Lagrangian and meshless code, based on SPH. In DualSPHysics, the fluid is discretized into a set of particles and the physical properties of each particle a are determined as an interpolation of the corresponding values of the neighboring particles. The contribution of each neighboring particle is weighed based on a kernel function that depends on the inter-distance between two particles (W) with a characteristic smoothing length (h).

2.3.1 *Governing equations in SPH*

The governing equations in SPH are the Navier-Stokes equations. Using the kernel function the N-S equation can be written in a discrete SPH Lagrangian system as:

$$\frac{d\rho_a}{dt} = \sum_b \boldsymbol{m}_b(\mathbf{v}_a - \mathbf{v}_b)\nabla_a W_{ab} \tag{13}$$

$$\frac{d\mathbf{v}_a}{dt} = -\sum_b \boldsymbol{m}_b\left(\frac{\boldsymbol{P}_b + \boldsymbol{P}_a}{\rho_b \cdot \rho_a} + \Pi_{ab}\right)\nabla_a W_{ab} + g \tag{14}$$

$$\frac{d\mathbf{r}_a}{dt} = \mathbf{v}_a \tag{15}$$

Where a is the target particle, b is the neighbour particle, t is time, $\mathbf{r}$ is the position, $\mathbf{v}$ is the velocity, $\boldsymbol{P}$ is the pressure, ρ is the density, m is the mass, and g is the acceleration of gravity and W_{ab} is the kernel function. In this study, the Quintic Kernel (Wendland 1995) function was adopted where the interaction between two particles a and b can be neglected after a distance of $2h$. Π_{ab} is the viscous term according to the artificial viscosity proposed in (Monaghan 1992). In DualSPHysics, the weakly compressible SPH formulation is used to solve the fluid. In addition, a Tait's equation of state is used to close the system:

$$P = \frac{c^2\rho_0}{\gamma}\left(\left(\frac{\rho}{\rho_0}\right)^\gamma - 1\right) \tag{16}$$

where ρ_0 is the reference fluid density, γ is the polytropic constant and c is the speed of sound. A more detailed description of the DualSPHysics formulation can be found in (Crespo et al. 2015).

2.3.2 *Boundary Conditions*

The standard method for DualSPHysics boundary conditions is the Dynamic Boundary Condition (DBC) (Crespo, Gómez-Gesteira, and Dalrymple 2007). In the DBC the boundary particles satisfy the same equations as the fluid particles however they do not move due to the forces exerted on them (or they move with an externally prescribed motion). When a fluid particle approaches a boundary particle and the distance between them is smaller than the kernel range, the density of the boundary particle is increased with a consequent increase in pressure. This results in a repulsive force being exerted on the fluid particle due to the pressure term in the momentum equation. The DBC has proven to be an efficient solution for engineering problems (Domínguez et al. 2015), however for some specific cases a large gap was created between the water particles and the boundary particles on transition zones between wet and not-wet areas. Recently, a novel methodology has been implemented in DualSPHysics: the modified Dynamic Boundary Conditions (mDBC) (English et al. 2021). The mDBC works with the same principle as the DBC, however the interaction boundary is defined between the outermost fluid and boundary particles. Thus, it is possible to mirror the boundary particles inside the fluid domain and using these mirrored ghost positions extrapolate the density of the solid particles evaluating the fluid particles and correct the SPH approximation when a fluid particle interacts with a boundary particle. The latter has been used in this research.

2.3.3 *Rigid Body Dynamics in DualSPHysics*

In DualSPHysics the motions of a rigid body are defined by calculating the interaction forces between fluid particles and floating boundary particles. The geometry of a floating body is discretized by filling its volume with boundary particles. The force on each boundary particle is then computed as a sum of the contribution of each surrounding fluid particle. Thus, each boundary particle k experiences a force per unit mass given by:

$$\boldsymbol{f}_k = \sum_a \boldsymbol{f}_{ka} \tag{17}$$

where f_{ka} is the force per unit mass exerted by the fluid particle a on the boundary particle k. For calculating the motions of the body, the standard equation of rigid body dynamics are applied:

$$\boldsymbol{M}\frac{d\mathbf{v}}{dt} = \sum m_k \boldsymbol{f}_k \tag{18}$$

$$\boldsymbol{I}\frac{d\boldsymbol{\Omega}}{dt} = \sum_k m_k(\boldsymbol{r}_k - \mathbf{R}_0) \times \boldsymbol{f}_k \tag{19}$$

where $\boldsymbol{M}$ is the total mass of the floating object, while $\boldsymbol{I}$ is the moment of inertia, $\mathbf{v}$ is the translational velocity, $\boldsymbol{\Omega}$ is the rotational velocity and $\mathbf{R}_0$ is the center of mass. Time integration of equations (18) and (19) is applied to predict the values of $\mathbf{v}$ and $\boldsymbol{\Omega}$ for the beginning of the next time step. Every boundary particle in the floating body consequently has a velocity given by:

$$\mathbf{v}_k = \mathbf{v} + \boldsymbol{\Omega}\,(\boldsymbol{r}_k - \boldsymbol{R}_0) \tag{20}$$

And all boundary particles within the floating body are finally moved with respect to the body center of mass by time integration of Eq. (20).

2.3.4 *Coupling with MoorDyn*

For simulating the mooring lines in this work the two-way coupling between DualSPHysics and MoorDyn+, which is a mooring library based on the original MoorDyn code, is used. A validation of the coupling was presented in (Domínguez et al. 2019). The coupled implementation is divided in three steps: i) the motions and rotations of the body ($\mathbf{v}, \boldsymbol{\Omega}$ and $\mathbf{R}_0$) are solved in DualSPHysics and used as input for the fairlead kinematics in the mooring library, ii) MoorDyn+ solves the mooring line behavior computing the forces in the fairlead connections and returning them to DualSPHysics ($d\mathbf{v}/\mathbf{dt}, \mathbf{d}\boldsymbol{\Omega}/\boldsymbol{dt}$) and iii) the forces are returned to DualSPHysics and used as external constraints to obtain the final positions and rotations of the rigid body. Note that MoorDyn+ coupled-to DualSPHysics does not include the effects of wave and current kinematics acting on the mooring line elements.

3 NUMERICAL SETUP

DeepCwind semi-submersible has undergone through many different iterations over the years. The version used in this paper is the first iteration tested in MARIN basin in 2011 (Goupee et al. 2012).

3.1 *Adapted-MoorDyn*

The difference of the first iteration compared to the later versions (Goupee et al. 2014; Robertson et al. 2017, 2020; Robertson, Jonkman, Masciola, et al. 2014) is the tower properties whereas the main dimensions of the platform remains the same in all versions. This changes the center of mass (CM) as well as platform's gross properties, which are summarized in Table 1.

Table 1. Semi-submersible platform properties

Quantity	Unit	Value
Total draft	m	20.0
Total mass	kg	13,444,000
Displacement	m^3	13,986.8
Roll inertia around CM	$kg \cdot m^2$	8.011×10^9
Pitch inertia around CM	$kg \cdot m^2$	8.011×10^9
Yaw inertia around CM	$kg \cdot m^2$	1.301×10^{10}
CM depth along centerline	m	14.4

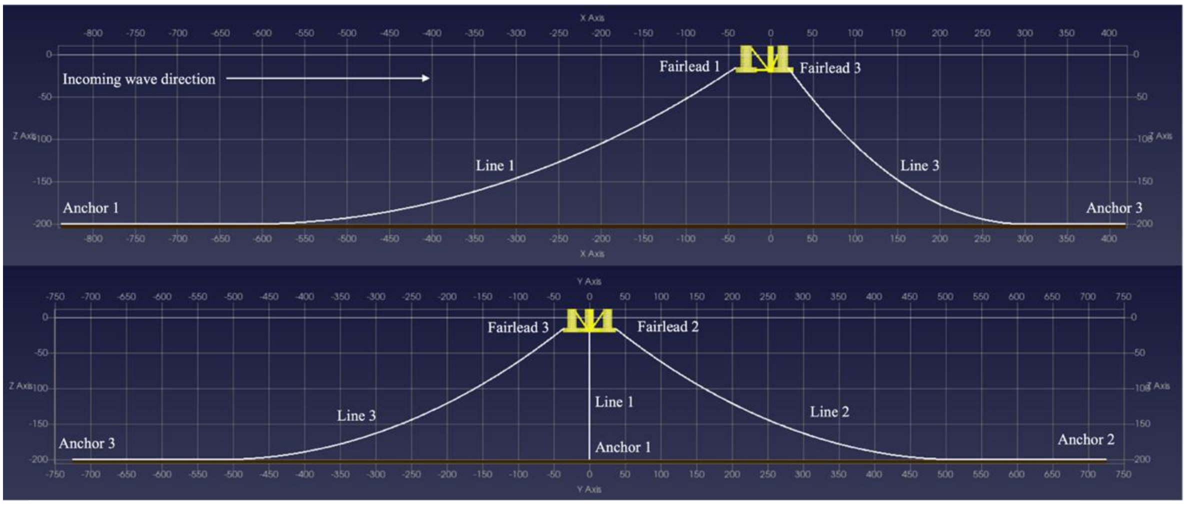

Figure 2. Mooring lines layout

Layout of the mooring configuration used in the numerical simulations is visualized in Figure 2 whereas the coordinates of the anchors and fairleads are shown in Table 2. The regular waves train comes from negative x-axis to the positive x direction. For this study, regular wave height (*H*) of 10.304 m with the wave period (*T*) of 12.1 s are chosen as defined in Hall & Goupee (2015) as Regular wave 5 Sea State with no wind-load applied.

Table 2. Anchor and fairlead positions

Anchor	**x (m)**	**y (m)**	**z (m)**
1	-837.6	0.0	-200.0
2	418.8	725.4	-200.0
3	418.8	-725.4	-200.0
Fairlead	**x (m)**	**y (m)**	**z (m)**
1	-40.87	0.0	-14.0
2	20.434	35.39	-14.0
3	20.434	-35.39	-14.0

Table 3. Mooring line properties

Quantity	**Unit**	**Value**
Equivalent diameter	m	0.134
Mass per 1 meter length	kg/m	116.600
Equiv. axial stiffness	N	753.6×10^6
Unstretched length line 1	m	833.6
Unstretched length line 2	m	834.8
Unstretched length line 3	m	834.85
Transverse drag coefficient	-	1.080
Tangential drag coefficient	-	0.213
Transverse added mass coeff.	-	0.865
Tangential added mass coeff.	-	0.269

Pretension is applied to each mooring line during the experiment, however, the pretension in Line 2 and Line 3 are not the same. For this reason, the unstretched length of the lines are adapted in the numerical simulation to match the pretension in the ocean basin test. Hence, the properties of the mooring lines used in this study are calibrated according to the one in Hall and Goupee (2015) instead of the original lengths defined in A. Robertson, Jonkman, Masciola, et al. (2014). These properties are shown in Table 3. The geometry used for the frequency-domain calculations is adapted from the example mesh provided by Orcina (2022). Adaptations are done in Rhinoceros® (McNeel & Others 2020) to include diagonal bracings. Additionally, a mesh refinement is performed using Gmsh (Geuzaine & Remacle 2009). The platform's geometry is according to the dimensions described in the OC4 project (Robertson, et al. 2014). Figure 3 shows the comparison of the geometry before (top) and after the adaptations (bottom).

Viscous effect is included by using the combination of Morison equation and quadratic damping shown in the Eq. (12). In surge, viscous force is due to the total frontal area of all the vertical cylinder members in YZ projection shown in Figure 2 (bottom). As for the heave, the projected area are calculated only for the bottom circular area of the large heave plates. The coefficients are taken from the values derived in Robertson, et al. (2014). In pitch, quadratic drag is modeled using the quadratic damping coefficient found in Coulling et al. (2013). These properties are summarized in Table 4.

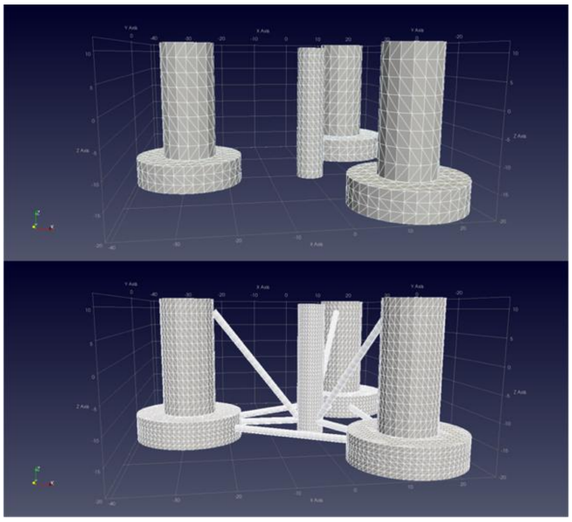

Figure 3. Orcina example (top) and modified mesh (bottom)

Table 4. Variables used to model the viscous force

Quantity	**Unit**	**Value**
A_1	m^2	1066
A_3	m^2	1357
C_{D_1}	$-$	0.632
C_{D_3}	$-$	4.8
B_5^v	Nms^2/rad^2	3.35×10^{10}

3.2 *DualSPHysics*

In DualSPHysics the DeepCWind test case presented in Section 3.1 has been simulated using a numerical wave flume with length of 800 m, width of 150 m and a water depth of 100 m. A piston-type wave generation was set at the left-hand side of the numerical flume and a numerical dissipative beach is located at the right hand-side to prevent wave reflection. Additionally, periodic boundaries and numerical damping are present at the top and bottom sides of the numerical flume to absorb the radiated and diffracted waves. The water depth was decreased from 200 m to a minimum of 100 m to achieve the same wave conditions as in the experiment while keeping the number of particles of the numerical flume limited.

The rigid body implemented in DualSPHysics corresponds to the adapted geometry. However, note that to keep the computational time reasonable the truss members were not filled with particles. After a convergence study, the inter-distance between two particles (dp) was set to dp = 0.8 m. Therefore, when using the mDBC boundary conditions the minimum number of particles inside these elements will not be met. Consequently the mass of the turbine was adjusted to achieve a draft of 20 m as in the experiment. Finally the mooring lines were defined using the same parameters as indicated in sub-section 3.1.

4 RESULTS AND DISCUSSIONS

In this section, the simulation results from Adapted-MoorDyn and DualSPHysics are compared with data from the experiment conducted in MARIN in 2011. The motions are with respect to the center of the domain (0,0,0) shown in Figure 2 where the calm water elevation is located at z = 0. The model tests results are digitized from the figures in Hall and Goupee (2015) using an open-source software called WebPlotDigitizer (Rohatgi 2021). Figure 4 and Figure 5 show the sensitivity analysis performed to investigate the influence of line discretization and time steps used in the simulation in the Adapted-MoorDyn. These two variables affect computational time linearly, thus, finding the balance between accuracy while maintaining computational efficiency is important in developing a time-efficient software. Figure 4 shows the comparison of fairleads' tension for three different line discretization. While fairlead 1 sees no difference in tension, increasing the segment number to 40 and 60 does slightly change the peak tension of fairlead 2 and fairlead 3. The same trend can be seen when observing the influence of time steps as shown in Figure 5 where the changes in peak tension of fairleads are less noticeable. In this case, running the simulation at 0.8 ms is preferable when considering the computational gain with not much accuracy improvement when going to a lower time steps.

Figure 9 show the results for the DeepCWind motions in surge, heave and pitch. For surge motion it can been seen that both Adapted-MoorDyn and DualSPHysics are capturing the surge motion correctly. During the experiments it was noticed that the surge motion is highly influenced by a viscous drift force. By considering the Morison equation in the Adapted-MoorDyn the time-varying wave orbital velocities capturing the drift force acting on the rigid body is considered. In heave motion, DualSPHysics is able to properly capture the body motions despite not including the truss members. Adapted-MoorDyn provides a better general agreement than the coupled numerical model in Hall & Goupee (2015). However, the minimum amplitude of heave motion is underpredicted by 24 %. In pitch motion, the highest amplitude of pitch is overpredicted by 35%

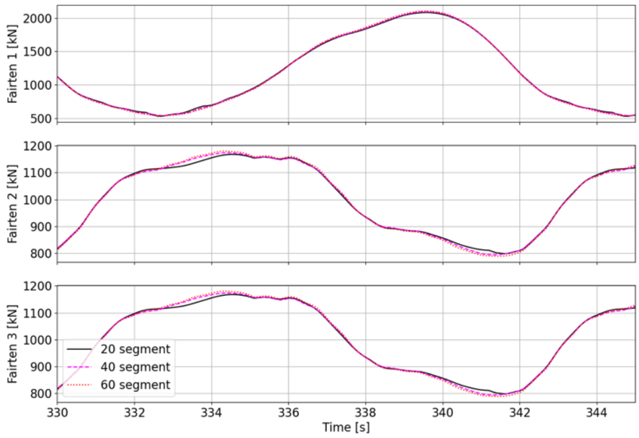

Figure 4. Influence of line discretization

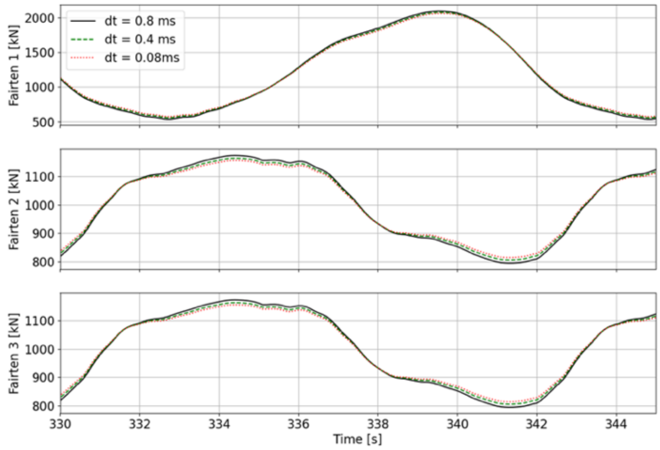

Figure 5. Influence of time steps

compared to the experiment for both Adapted-MoorDyn and DualSPHysics. Both numerical models excluded viscous effect from the diagonal members, which likely to be the reason for the discrepancies with results from the experiment. A phase shift is noticeable when observing pitch motions predicted by the Adapted-MoorDyn, but not in DualSPHysics. Figure 8 shows the fairlead tensions comparison between both numerical models and the experiments. For all fairleads, both Adapted-MoorDyn and DualSPHysics underpredicted the highest tensions by just less than 5 % . Nevertheless, the lowest tension in fairlead 1 is overpredicted by 75 % compared to the experiment for Adapted-MoorDyn and 85% for DualSPHysics. Finally, the lowest tension in farleads 2 and 3 is overpredicted in DualSPHysics by a 9%. The overprediction in the Adapted-MoorDyn can be due to not achieving the same slack in the numerical simulation as in the experiment as it can be inferred for the small disagreement in the heave motion and the phase shift in the pitch motion. For DualSPHysics the overprediction may be caused by the overestimation of the pitch motion.

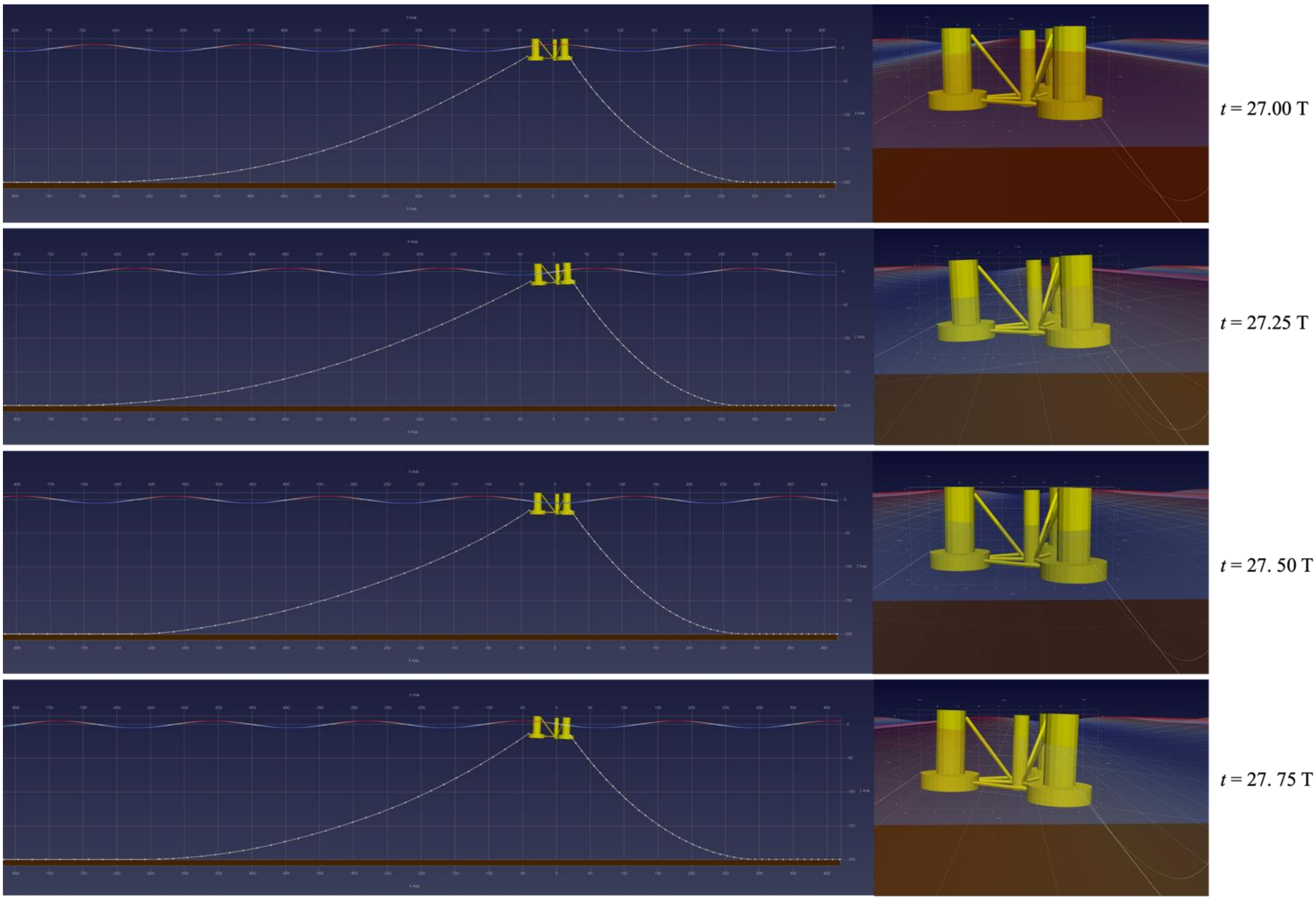

Figure 6. Snapshots of the simulation at t = 326.7s (27.00T) until t = 335.8 s (27.75T)

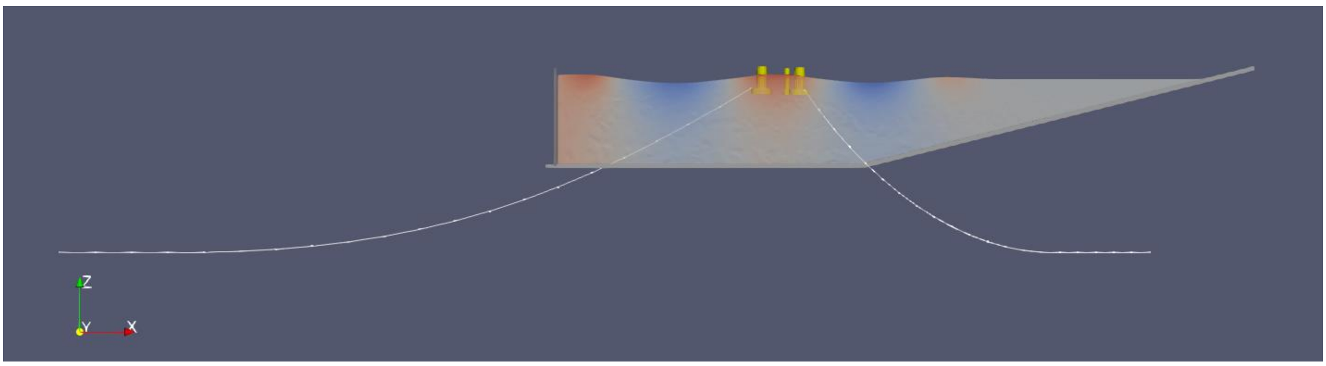

Figure 7. Snapshot of the DualSPHysics simulation domain

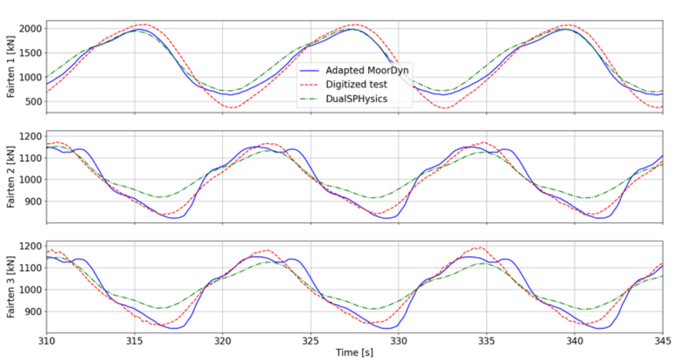

Figure 8. Fairleads' tension comparison

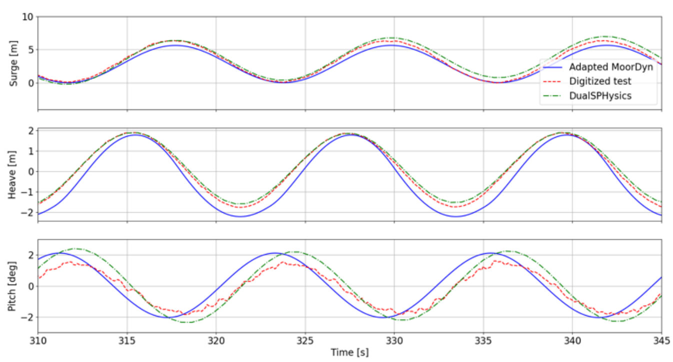

Figure 9. Platform's motion comparison

5 CONCLUSIONS AND FUTURE WORK

A time-efficient algorithm, Adapted-MoorDyn, capable of modelling the hydrodynamics of a floating wind turbine platform has been presented in this paper. Adapted-MoorDyn has been compared to the fully non-linear solver DualSPHysics and experimental results. The FWT motions and fairleads tensions have been studies. General agreement in terms of motions is found between Adapted-MoorDyn, DualSPHysics and the experiments except for pitch motions that are out-of-phase for Adapted-MoorDyn and overpredicted in DualSPHysics. The mooring line peak tensions in all fairleads are predicted well with the largest discrepancies of 5 % found in fairlead 1 for both numerical models. Nonetheless, lowest tension in the fairleads is overpredicted due to the discrepancies in pitch that have been observed for both models. Modelling the truss diagonal members would likely to solve this issue.

This investigation has shown that it is possible to replicate the same simulation in Adapted-MoorDyn and DualSPHysics under linear wave conditions and validated it. Future work will focus on establishing a methodology to use Adapted-MoorDyn to simulate multiple different mooring configuration layouts against different load cases to find the most cost-effective mooring design. Then, this mooring layout configuration will be simulated in DualSPHysics under extreme load conditions to ensure the integrity of the system under extreme load cases considering viscous effects, wave run-up and wave breaking. Additionally, further investigation will be performed to test the robustness of this algorithm against different wave conditions including the irregular wave cases.w.

REFERENCES

Airy, and G.B. 1841. “Tides and Waves.” *Encyclopaedia Metropolitana*.

Ancellin, M., and F. Dias. 2019. “Capytaine: A Python-Based Linear Potential Flow Solver.” *J. Open Source Softw* 4(36):1341.

Armesto, José A., Raúl Guanche, Fernandodel Jesus, Arantza Iturrioz, and Iñigo J. Losada. 2015. “Comparative Analysis of the Methods to Compute the Radiation Term in Cummins’ Equation.” *Journal of Ocean Engineering and Marine Energy* 1(4):377–93. doi: 10.1007/s40722-015-0027-1.

Coulling, Alexander J., Andrew J. Goupee, Amy N. Robertson, Jason M. Jonkman, and Habib J. Dagher. 2013. “Validation of a FAST Semi-Submersible Floating Wind Turbine Numerical Model with DeepCwind Test Data.” *Journal of Renewable and Sustainable Energy* 5(2). doi: 10.1063/1.4796197.

Crespo, A. J. C., J. M. Domínguez, B. D. Rogers, M. Gómez-Gesteira, S. Longshaw, R. Canelas, R. Vacondio, A. Barreiro, and O. García-Feal. 2015. “DualSPHysics: Open-Source Parallel {CFD} Solver Based on Smoothed Particle Hydrodynamics (SPH).” *Computer Physics Communications* 187:204–16. doi: http://dx.doi.org/10.1016/j.cpc.2014.10.004.

Crespo, A. J. C., M. Gómez-Gesteira, and R. A. Dalrymple. 2007. “Boundary Conditions Generated by Dynamic Particles in SPH Methods.” *Computers, Materials and Continua* 5(3):173–84.

Cummins, W. 1962. “The Impulse Response Function and Ship Motions.” *Schiffstechnik* 9:101–9.

Dagher, Habib, Anthony Viselli, Andrew Goupee, Jeffrey Thaler, Damian Brady, Peter Browne, James Browning, Jade Chung, Alexander Coulling, Heather Deese, Matthew Fowler, Rebecca Holberton, Jain Anant, Dustin Jalbert, Theresa Johnson, Jason Jonkman, Benjamin Karlson, Richard Kimball, Bonjun Koo, Matthew Lackner, Kostas Lambrakos, Matthew Lankowski, Adrienne Leopold, Ho-Joon Lim, Linda Mangum, Heather Martin, Marco Masciola, Melissa Maynard, James McCleave, Robert Mizrahi, Paul Molta, Andrew Pershing, Neal Pettigrew, Ian Prowell, Andrew Qua, Graham Sherwood, Thomas Snape, Robert Steneck, Gordon Stewart, Jason Stockwell, Andrew H. P. Swift, Dale Thomas, Elizabeth Viselli, and Gayle Zydlewski. 2013. *Final Technical Report. DeepCwind Consortium Research Program. January 15, 2010 - March 31, 2013*. Vol. 1. Golden, CO (United States).

Domínguez, J. M., A. J. C. Crespo, J. L. Cercos-Pita, G. Fourtakas, B. D. Rogers, and R. Vacondio. 2015. “Evaluation of Reliability and Efficiency of Different Boundary Conditions in an SPH Code.” in *Proceedings of the 10th SPHERIC International Workshop*. Parma, Italy.

Domínguez, J. M., G. Fourtakas, C. Altomare, R. B. Canelas, A. Tafuni, O. García-Feal, I. Martínez-Estévez, A. Mokos, R. Vacondio, A. J. C. Crespo, B. D. Rogers, P. K. Stansby, and M. Gómez-Gesteira. 2021. “DualSPHysics: From Fluid Dynamics to Multiphysics Problems.” *Computational Particle Mechanics*. doi: 10.1007/s40571-021-00404-2.

Domínguez, José M., Alejandro J. C. Crespo, Matthew Hall, Corrado Altomare, Minghao Wu, Vasiliki Stratigaki, Peter Troch, Lorenzo Cappietti, and Moncho Gómez-Gesteira. 2019. “SPH Simulation of Floating Structures with Moorings.” *Coastal Engineering* 153(November 2018). doi: 10.1016/j.coastaleng.2019.103560.

Duclos, Gaelle, Alain H. Clément, and Gontran Chatry. 2001. “Absorption of Outgoing Waves In a Numerical Wave Tank Using a Self-Adaptive Boundary Condition.” *International Journal of Offshore and Polar Engineering* 11(3).

English, A., J. M. Domínguez, R. Vacondio, A. J. C. Crespo, P. K. Stansby, S. J. Lind, L. Chiapponi, and M. Gómez-Gesteira. 2021. “Modified Dynamic Boundary Conditions (MDBC) for General-Purpose Smoothed Particle Hydrodynamics (SPH): Application to Tank Sloshing, Dam Break and Fish Pass Problems.” *Computational Particle Mechanics*. doi: 10.1007/s40571-021-00403-3.

Fenton, J. D. 1988. “The Numerical Solution of Steady Water Wave Problems.” *Computers and Geosciences* 14(3):357–68. doi: 10.1016/0098-3004(88)90066-0.

Fernandez, G., A. Pribadi, W. Minghao, V. Stratigaki, P. Troch, and E. Lataire. 2021. “Experimental Validation of a State Space Model of a Moored Cuboid in Waves.” in *14th European Wave and Tidal Energy Conference (EWTEC 2021)*. Plymouth: 14th European Wave and Tidal Energy Conference.

Geuzaine, Christophe, and Jean-François Remacle. 2009. “Gmsh: A 3-D Finite Element Mesh Generator with Built-in Pre- and Post-Processing Facilities.” *International Journal for Numerical Methods in Engineering* 79(11):1309–31. doi: 10.1002/nme.2579.

Goupee, Andrew J., Richard W. Kimball, Joop Helder, and Matthew J. Fowler. 2014. “ADDITIONAL WIND/WAVE

BASIN TESTING OF THE DEEPCWIND SEMI-SUBMERSIBLE WITH A PERFORMANCE-MATCHED WIND TURBINE Andrew." Pp. 1–10 in. Proceedings of the ASME 2014 33rd International Conference on Ocean, Offshore and Arctic Engineering.

Goupee, Andrew J., Bonjun J. Koo, Kostas F. Lambrakos, and Richard W. Kimball. 2012. "Model Tests for Three Floating Wind Turbine Concepts." *Offshore Technology Conference, Proceedings* 3:2584–99. doi: 10.4043/23470-ms.

Gueydon, Sébastien, Tiago Duarte, and Jason Jonkman. 2014. "Comparison of Second-Order Loads on a Semisubmersible Floating Wind Turbine." *Proceedings of the International Conference on Offshore Mechanics and Arctic Engineering - OMAE* 9A(March). doi: 10.1115/OMAE2014-23398.

Hall, Matthew. 2017. *MoorDyn User's Guide*.

Hall, Matthew, and Andrew Goupee. 2015. "Validation of a Lumped-Mass Mooring Line Model with DeepCwind Semisubmersible Model Test Data." *Ocean Engineering* 104:590–603. doi: 10.1016/j.oceaneng.2015.05.035.

Herzig, Gunnar. 2022. *Global Offshore Wind Report 2021*.

Jonkman, Jm, S. Butterfield, W. Musial, and G. Scott. 2009. *Definition of a 5-MW Reference Wind Turbine for Offshore System Development*.

Koo, Bonjun J., Andrew J. Goupee, Richard W. Kimball, and Kostas F. Lambrakos. 2014. "Model Tests for a Floating Wind Turbine on Three Different Floaters." *Journal of Offshore Mechanics and Arctic Engineering* 136(2):1–11. doi: 10.1115/1.4024711.

Lee, Joyce, and Feng Zhao. 2021. *GWEC Global Wind Report*.

Liu, Yuanchuan, Qing Xiao, Atilla Incecik, Christophe Peyrard, and Decheng Wan. 2017. "Establishing a Fully Coupled CFD Analysis Tool for Floating Offshore Wind Turbines." *Renewable Energy* 112:280–301. doi: 10.1016/j.renene.2017.04.052.

McNeel, R., and Others. 2020. "Rhinoceros 3D."

Monaghan, J. J. 1992. "Smoothed Particle Hydrodynamics." *Annual Review of Astronomy and Astrophysics* 30(1):543–74. doi: 10.1146/annurev.aa.30.090192.002551.

Morison, J. R., M. P. O'Brien, J. W. Johnson, and S. A. Schaaf. 1950. "The Force Exerted by Surface Waves on Piles." *Journal of Petroleum Technology* 22(3):359–67. doi: 10.2118/950149-G.

Ogilvie, T. 1964. "Recent Progress toward the Understanding and Prediction of Ship Motions." Pp. 3–80 in *5th Symposium on Naval Hydrodynamics*. Bergen.

Orcina. 2022. "Orcaflex Examples." Retrieved (https://www.orcina.com/SoftwareProducts/OrcaFlex/Examples/).

Pillai, Ajit C., Philipp R. Thies, and Lars Johanning. 2019. "Mooring System Design Optimization Using a Surrogate Assisted Multi-Objective Genetic Algorithm." *Engineering Optimization* 51(8):1370–92. doi: 10.1080/0305215X.2018.1519559.

Press, William H., Saul a Teukolsky, William T. Vetterling, and Brian P. Flannery. 2007. *Numerical Recipes 3rd Edition: The Art of Scientific Computing*.

Pribadi, A. B. K., L. Donatini, and E. Lataire. 2019. "Numerical Modelling of a Mussel Line System by Means of Lumped-Mass Approach." *Journal of Marine Science and Engineering* 7(9). doi: 10.3390/jmse7090309.

Ramírez, Lizet, Daniel Fraile, Guy Brindley, and Rory O'Sullivan. 2021. "Offshore Wind in Europe: Key Trends and Statistics 2020." in *WindEurope*.

Robertson, A. N., S. Gueydon, E. Bachynski, L. Wang, J. Jonkman, D. Alarcón, E. Amet, A. Beardsell, P. Bonnet, B. Boudet, C. Brun, Z. Chen, M. Féron, D. Forbush, C. Galinos, J. Galvan, P. Gilbert, J. Gómez, V. Harnois, F. Haudin, Z. Hu, J. Le Dreff, M. Leimeister, F. Lemmer, H. Li, G. McKinnon, I. Mendikoa, A. Moghtadaei, S. Netzband, S. Oh, A. Pegalajar-Jurado, M. Q. Nguyen, K. Ruehl, P. Schünemann, W. Shi, H. Shin, Y. Si, F. Surmont, P. Trubat, J. Qwist, and S. Wohlfahrt-Laymann. 2020. "OC6 Phase I: Investigating the Underprediction of Low-Frequency Hydrodynamic Loads and Responses of a Floating Wind Turbine." *Journal of Physics: Conference Series* 1618(3). doi: 10.1088/1742-6596/1618/3/032033.

Robertson, Amy, Jason Jonkman, M. Masciola, H. Song, A. Goupee, A. Coulling, and C. Luan. 2014. "Definition of the Semi-Submersible Floating System for Phase II of OC4." (September).

Robertson, Amy, Jason Jonkman, Fabian Vorpahl, Wojciech Popko, Jacob Qvist, Lars Frøyd, Xiaohong Chen, José Azcona, Emre Uzunoglu, Carlos Guedes Soares, Chenyu Luan, Huang Yutong, Fu Pengcheng, Anders Yde, Torben Larsen, James Nichols, Ricard Buils, Liu Lei, Tor Anders Nygaard, Dimitris Manolas, Andreas Heege, Sigrid Ringdalen Vatne, Harald Ormberg, Tiago Duarte, Cyril Godreau, Hans Fabricius Hansen, Anders Wedel Nielsen, Hans Riber, Cédric Le Cunff, Friedemann Beyer, Atsushi Yamaguchi, Kwang Jin Jung, Hyunkyoung Shin, Wei Shi, Hyunchul Park, Marco Alves, and Matthieu Guérinel. 2014. "Offshore Code Comparison Collaboration Continuation within IEA Wind Task 30: Phase II Results Regarding a Floating Semisubmersible Wind System." in *Proceedings of the International Conference on Offshore Mechanics and Arctic Engineering - OMAE*. Vol. 9B.

Robertson, Amy N., Fabian Wendt, Jason M. Jonkman, Wojciech Popko, Habib Dagher, Sebastien Gueydon, Jacob Qvist, Felipe Vittori, José Azcona, Emre Uzunoglu, Carlos Guedes Soares, Rob Harries, Anders Yde, Christos Galinos, Koen Hermans, Jacobus Bernardus de Vaal, Pauline Bozonnet, Ludovic Bouy, Ilmas Bayati, Roger Bergua, Josean Galvan, Iñigo Mendikoa, Carlos Barrera Sanchez, Hyunkyoung Shin, Sho Oh, Climent Molins, and Yannick Debruyne. 2017. "OC5 Project Phase II: Validation of Global Loads of the DeepCwind Floating Semisubmersible Wind Turbine." *Energy Procedia* 137:38–57. doi: 10.1016/j.egypro.2017.10.333.

Rohatgi, Ankit. 2021. "WebPlotDigitizer."

Sheng, W., R. Alcorn, and A. Lewis. 2015. "A New Method for Radiation Forces for Floating Platforms in Waves." *Ocean Eng.* 105:43–53.

Wang, Lu, Amy Robertson, Jason Jonkman, Jang Kim, Zhi Rong Shen, Arjen Koop, Adrià Borràs Nadal, Wei Shi, Xinmeng Zeng, Edward Ransley, Scott Brown, Martyn Hann, Pranav Chandramouli, Axelle Viré, Likhitha Ramesh Reddy, Xiang Li, Qing Xiao, Beatriz Méndez López, Guillén Campaña Alonso, Sho Oh, Hamid Sarlak, Stefan Netzband, Hyunchul Jang, and Kai Yu. 2022. "OC6 Phase Ia: CFD Simulations of the Free-Decay Motion of the DeepCwind Semisubmersible." *Energies* 15(1). doi: 10.3390/en15010389.

Wendland, Holger. 1995. "Piecewise Polynomial, Positive Definite and Compactly Supported Radial Functions of Minimal Degree." *Advances in Computational Mathematics* 4(1):389–96. doi: 10.1007/BF02123482.

Wheeler, J. D. 1970. "Method for Calculating Forces Produced by Irregular Waves." *Journal of Petroleum Technology* 22(3):359–67. doi: 10.2118/2712-pa.